TEMPORAL TREATMENT OF A THERMAL RESPONSE FOR DEFECT DEPTH ESTIMATION

Y. A. Plotnikov and W. P. Winfree
MS 231
NASA Langley Research Center
Hampton, VA 23681-0001

INTRODUCTION

Transient thermography, which employs pulse surface heating of an inspected component followed by acquisition of the thermal decay stage, is gaining wider acceptance as a result of its remoteness and rapidness. Flaws in the component's material may induce a thermal contrast in surface thermograms. An important issue in transient thermography is estimating the depth of a subsurface flaw from the thermal response. This improves the quantitative ability of the thermal evaluation: from one scan it is possible to locate regions of anomalies in thickness (caused by corrosion) and estimate the implications of the flaw on the integrity of the structure.

Our research focuses on thick composite aircraft components. A long square heating pulse and several minutes observation period are required to receive an adequate thermal response from such a component. Application of various time-related informative parameters of the thermal response for depth estimation is discussed. A three-dimensional finite difference model of heat propagation in solids in Cartesian coordinates is used to simulate the thermographic process. Typical physical properties of polymer graphite composites are assumed for the model.

PROCESSING OF THE THERMAL RESPONSE IN TIME DOMAIN

To estimate a defect's depth, the most widely used algorithms utilize temporal characteristics of the thermal response received from the excited surface. Algorithms parameterize the flaw depth in terms of a specified point on the thermal contrast curve or a divergence point between two temperature evolution curves from a characteristic thermal response (flawless material) and an inspected area. Application of this approach requires satisfactory completion of two successive tasks. The first is obtaining a smooth thermal contrast curve for each pixel in a thermal image. Calculating the thermal contrast involves extracting two temperature time-evolutions: for an inspected and reference point ($T(t)$ and

$T_{ref}(t)$ respectively). Then the second task of characteristic point locating is solved. By measuring the time of this point on each thermal contrast curve $C(t)$, it is possible to construct a new image with improved defect characterization. Since several characteristic points are commonly used to characterize the depth of the flaw, from one thermal contrast curve, it is possible to construct several characteristic images.

COMPARISON OF THE ALGORITHMS (COMPUTATIONAL APPROACH)

Three time evolution functions of a thermal response acquired from a composite specimen with known flaws are presented in Fig. 1a. The signal $T_{ref}(t)$ is the average of the thermal response in a reference region. $T_3(t)$ and $T_5(t)$ are the averaged thermal response for regions above flat bottom holes located 3 and 5 mm under the specimen surface. The curves for defect depth of 3 and 5 mm are noticeably deviated from $T_{ref}(t)$ during the measurement time interval. Therefore there is a sufficient thermal contrast and it is possible to quantitatively characterize those defects.

A common form for a thermal contrast function is given by the expression

$$C(t) = \frac{T(t) - T_{ref}(t)}{T_{ref}(t)}. \qquad (1)$$

Fig. 1b shows the thermal contrast $C_3(t)$ smoothed with a low pass filter to reduce the noise. Several characteristic points on the contrast curve have been identified as parameters enabling defect depth estimation. One of the earliest time points on a temperature time evolution curve that is used for defect depth characterization is a moment of time when the temperature signal above the inspected point diverges from the reference signal (Fig. 1a). Establishing of a threshold level is required to identify this point on a time evolution curve [1]. The corresponding parameter t_{div} on the thermal contrast curve can be defined as the time when $C(t)$ crosses a specified threshold level (Fig. 1b). Another early time point is the moment when the contrast curve has the peak slope [2]. This parameter, t_{ps}, is easily to find by seeking the maximum of the first derivative of the thermal contrast time evolution function.

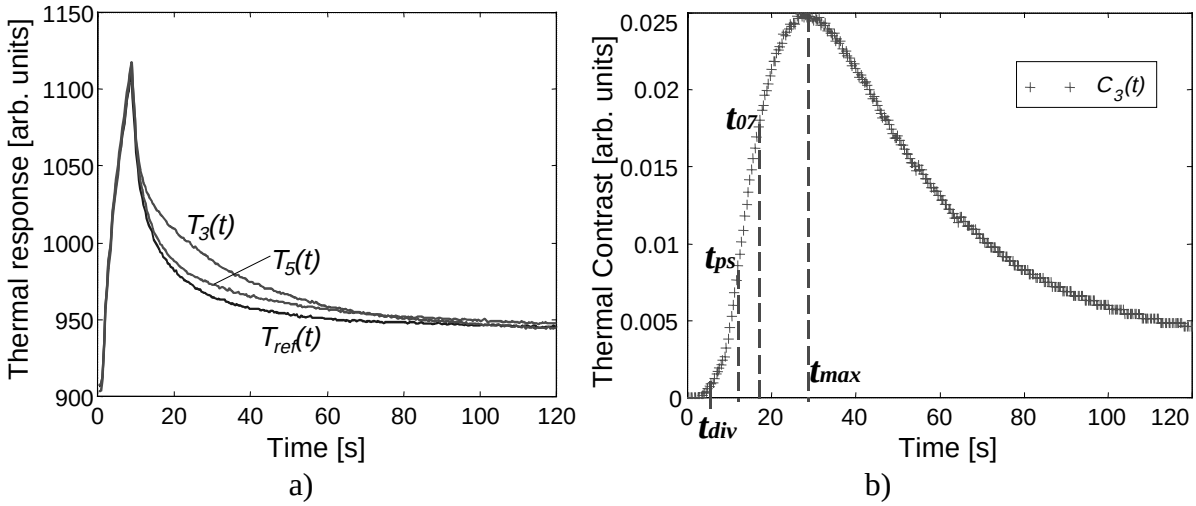

a) b)

Figure 1. Time evolution functions of the thermal response (a) and thermal contrast (b).

A later time interval is also commonly used for defect depth estimation. Several characteristic points are linked to the moment when the thermal contrast reaches its maximum. The time of maximum, t_{max}, and the moment when the contrast crosses a level which is a portion of its maximum are the examples of such characteristics. Particularly, the time interval corresponding to the contrast reaching 0.72 of the maximum contrast value, t_{07}, has been reported as more stable and accurate than t_{max} [3], and is considered in our investigation.

The purpose of this work is to perform a fair comparison of these informative parameters and highlight their strengths and weaknesses. Thermal contrast extraction from noisy experimental data is a complicated procedure requiring a careful application of reduction techniques. For this reason, it is informative to study general features of the mentioned characteristic points using noise-free simulated thermal contrast curves. This approach helps to assess their behavior without biasing a particular contrast computation algorithm. Work with simulated thermograms enables determination of a reference (defect free) response computation more easily because the configuration of the modeled structure is known. Computed thermal contrast functions are smooth. Therefore, informative parameters can be determined invariantly. Moreover, it is possible to simulate a low amplitude thermal signal, which is non-resolvable with the existing apparatus setup.

Cross sections at the centerline of three-dimensional models that are used for numerical computations are presented in Fig. 2. An isotropic plate of 100x100x20 mm^3 (Fig. 2a) is used to investigate the parameters of interest. Thermal properties of the media are chosen to represent a composite material (thermal diffusivity $\alpha = 1.4 \cdot 10^{-6} m^2 / s$, thermal conductivity $K = 2.7 W / m \cdot K$). The defect incorporated into the model is a square non-conductive flat-bottom void with 20 mm on a side. The bottom of the void is located at a depth d below the surface (Fig. 2a). An instantaneous uniformly distributed heating pulse is used to excite the upper surface. An alternating direction implicit scheme is used to obtain a solution of the 3D thermal diffusion equation. Boundary conditions are chosen to simulate an adiabatic transient process. Temperature evolution functions are computed at the central point of the plate (above the center of the flaw) and at the corner of the plate (for the reference value). The time evolution of the thermal contrast is computed by the equation (1) from these two temperature functions.

The time-related parameters of the obtained thermal contrast curves have been computed with d varied from 1 to 19 mm. The results are shown in Fig. 3a. All considered

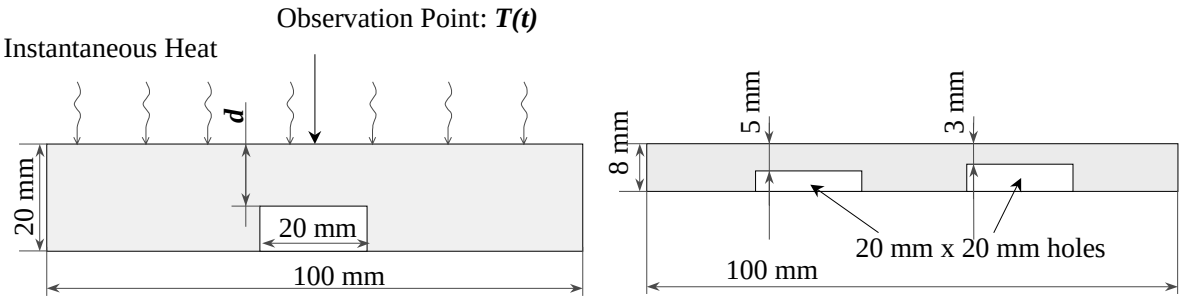

a) b)

Figure 2. Models for simulations. a) isotropic panel with one defect; b) anisotropic panel with 2 defects.

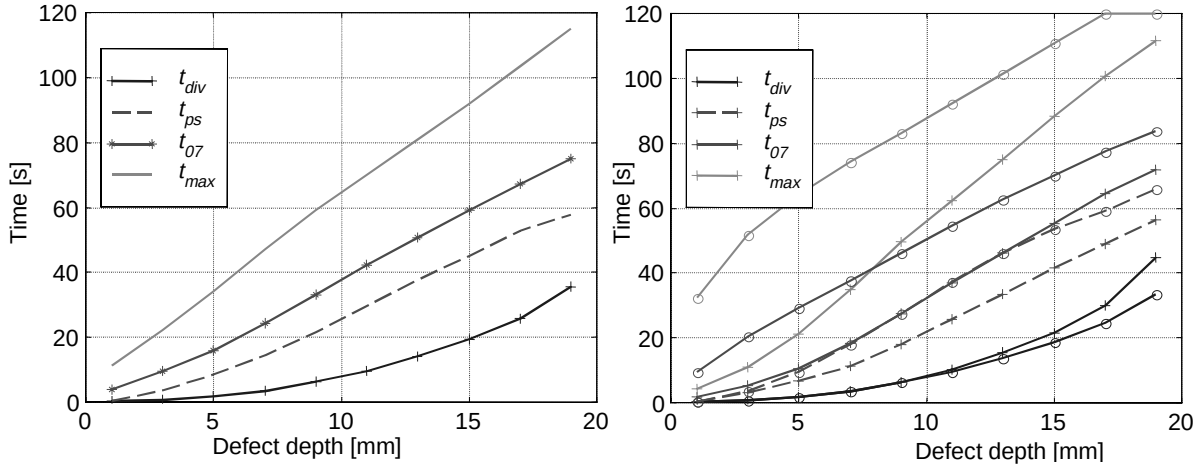

Figure 3. Temporal informative parameters for variable depth of a square non-conductive void (data from simulated thermal contrast evolutions). a) defect size is 20x20 mm^2 ; b) defect size is 10x10 mm^2 (shown in +-+-+) and 40x40 mm^2 (shown in o-o-o).

parameters are dependent on the defect depth variations and therefore can be used for defect depth estimation. The curve $t_{div}(d)$ has a parabola-like shape while other characteristics are closer to linear functions. Defect size variations impact the parameter's behavior. Fig. 3b contains the same characteristic times for defect sizes 0.5 and 2.0 of the plate's thickness (10x10 mm^2 and 40x40 mm^2 respectively). The earliest time parameters (t_{div} and t_{ps}) are approximately independent of flaw size for shallow defects and differ significantly only for deeper defects. In contrast, $t_{\max}$ and t_{07} have a large dependence on flaw size for shallow depths. Our model approximates the thermographic technique by adiabatic boundary condition, therefore the structure above a wide defect approximates a thermally insulated plate of thickness *d* for the initial period after heat application. For a one-dimensional case, the contrast never achieves a maximum; therefore the timing of the maximum is a function of both the size and depth of the flaw.

The next phase of the simulation is obtaining lateral profiles of these time-related parameters above defects. It is informative for comparison of different techniques to simulate two defects in close proximity. The model configuration for this case is shown in Fig. 2b. Anisotropic media is considered (for in-depth direction $\alpha = 0.7 \cdot 10^{-6} m^2 / s$; in-plane thermal diffusivities are $1.8 \cdot 10^{-6} m^2 / s$ and $1.4 \cdot 10^{-6} m^2 / s$ along and across the defect centerline respectively). The parameters of this model were set to fit the physical conditions of the measurements described in the next section.

Two-dimensional distributions were obtained for all informative parameters from the simulated thermal response. The lateral profiles above two voids located 5 and 3 mm under the surface are presented in Fig. 4a. Presence of both defects is evident in the reduced values of the characteristic times. The curves characterize the defect-plate boundary of the shallow defect more accurately (flat part with less visible noise) than the deeper one. The t_{ps} profile is noisier than the others. A series of simulated thermal images were stored in a binary format with a limited dynamic range to accurately represent the measurement. This results in introduction of noise into the time derivative, an effect that is quite similar to experimental results. It is also noticeable that the late time parameters: t_{07} and $t_{\max}$ provide better lateral

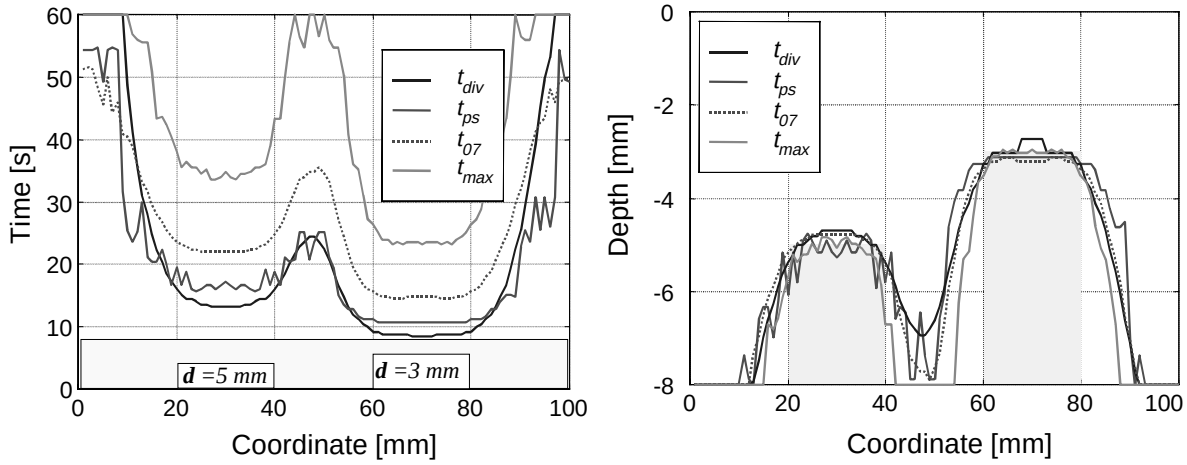

a) b)

Figure 4. Characteristic time profiles (a) and depth profiles (b) obtained from a simulated data set.

separation of the defects. This can be explained by their better in-depth penetration.

To characterize the defect depth a simple data inversion procedure is applied using a polynomial of kind

$$d = a\sqrt{t_{char}} + b \cdot t_{char} + c\,, \qquad (2)$$

where t_{char} is one of the temporal informative parameters used. The constants *a*, *b*, and *c* have been determined for each informative parameter separately. The estimated depth profiles and the actual geometry of the voids are shown in Fig. 4b. The obtained bottom profiles accurately depict the defect top, but overestimate the lateral size of the voids.

Variations of the defect depth in a wide range have highlighted some expected limitations of the techniques. For example, it is difficult to obtain a depth profile based on t_{div} parameter for shallow (depth is less than 2 mm) defects. The depth estimations based on $t_{\max}$ parameter have a noticeable crater-like surface for shallow defects (effect of the defect size variation is shown in Fig. 3b). The deep (depth is greater than 6 mm) defects cause noisy profiles estimated from t_{ps}, while for other parameters, deep defects result in more rounded estimated profiles for the defect.

COMPARISON OF THE ALGORITHMS (EXPERIMENTAL APPROACH)

Experimental validation of results obtained with numerical simulations is very important. Composite specimens and measurement systems hardware add undesired artifacts to a thermal signal. Therefore, they can be considered as factors that reduce a technique's capability for accurate characterization of a structure. Since these distortions are complicated in nature, it is more suitable to assess the data processing techniques with experimentally obtained data rather than to attempting to simulate the distortions. Measurements have been performed on a piece of an aircraft wing box structure composed of thick stitched graphite-epoxy composite polymer. The panel has a nominal thickness of 8 mm with 5 flat bottom 20x20 mm^2 holes machined into the backside. A thermal flux pulse lasting 8.5 seconds is applied to the front by two quartz lamps with a total power of 1.5 kW. A series of 150

thermal images of 256x256 elements each with a sampling rate of 2.5 Hz is acquired for post processing.

As was mentioned earlier, the thermal contrast is often computed before extracting quantitative information from experimental data. It is notable that there are several equations for calculating the thermal contrast. Three commonly used functions for calculation of the thermal contrast for a single pixel in the image were considered[4, 5]:

$$C(t) = \frac{T(t) - T_{ref}(t)}{T_{ref}(t) - T_{ref}(0)}; \tag{3}$$

$$C(t) = \frac{T(t) - T(0)}{T_{ref}(t) - T_{ref}(0)}; \tag{4}$$

$$C(t) = \frac{T(t) - T(0)}{T(t_h) - T(0)} - \frac{T_{ref}(t) - T_{ref}(0)}{T_{ref}(t_h) - T_{ref}(0)}, \tag{5}$$

where t_h is the time of the heating pulse (the moment of time when thermal response has the highest magnitude). Although it was possible to identify the defects in all distributions $t_{char}(i, j)$, the eq. 3 provides the poorest result while the thermal contrast normalized by the signal peak value (computed by eq. (5)) provides the clearest defect images in the timegrams. They are presented in Fig. 5. It worth noting that a time evolution function can be constructed for a segment of several (for instance 3x3) pixels. This furnishes a lower noise level and offers more possibilities for the contrast computation (see [6] for example) . However, this increase in the number of possible permutations makes it difficult to compare the contrast extraction techniques.

To compute the depth of the defects, eq. (2) is applied to the obtained characteristic time distributions. The estimated depth profile obtained from t_{div} yields an inaccurate

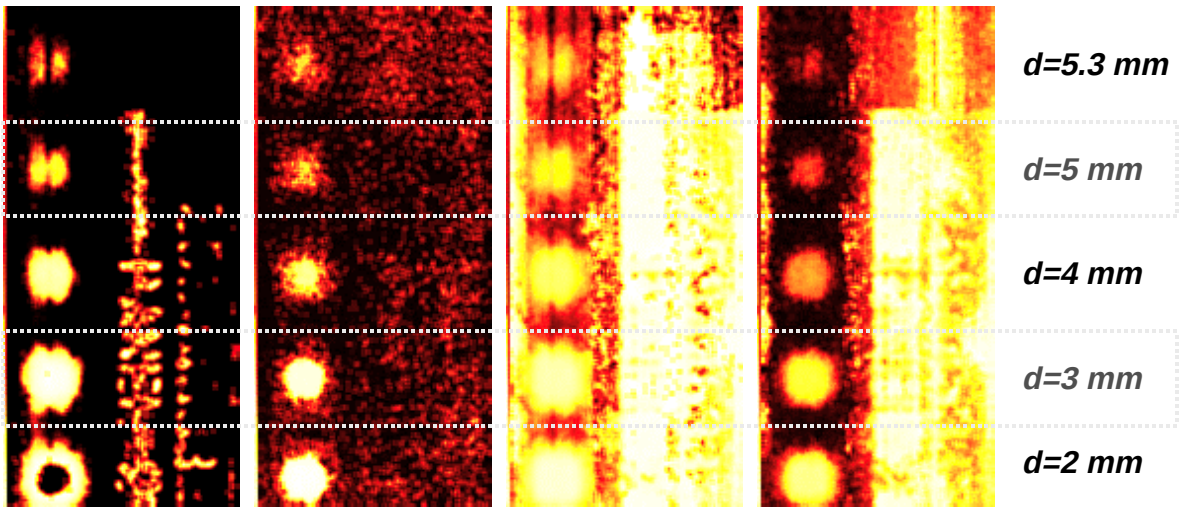

Figure 5. Timegrams $t_{char}(i, j)$ of the 8 mm composite panel with flat bottom holes of various depths obtained by using different informative parameters. a) t_{div}; b) t_{ps}; c) t_{07}; d) $t_{\max}$.

representation of the shallowest defect (Fig. 5a) which indicates the difficulties of applying this technique to shallow defects. A gray scale depth image obtained by averaging the depth profiles estimated from the three other timegrams is shown in Fig. 6a. Fig. 6b demonstrates a comparison between the estimated and actual (dotted line) bottom profiles for the centerline of the defects. The reconstructed profiles for the defects have rounded edges. Also the noise in the area with no defects is noticeable in Fig. 6a. To correct the results shown in Fig. 6a, an initial defect map is constructed from the thermal response of the specimen using a procedure that has been explained in detail elsewhere [7]. It uses the pulse phase technique followed by the Laplacian defect shape extraction routine. The defect planar geometry in the resulting defect map has been shown to give a much more accurate representation of the real defect geometry. A masking of the depth profile with this binary defect map yields an accurate representation of the internal structure. The 3D representation of this result is shown in Fig. 7. This figure demonstrates the significant potential of the thermal pulse technique for defect visualization and quantification in composites.

CONCLUSION

For large defects (lateral sizes greater than double the thickness of the panel) located at the middle of a composite panel, all considered informative parameters have been found suitable for defect depth estimation. The best results were obtained by averaging the depth profiles obtained based on several characteristic points on the thermal contrast curves. Clearly, some care must be taken when using the earliest time parameters (t_{div}, t_{ps}) for shallow defect depth estimation. Accurate characterization of these parameters requires a sampling rate which is high enough to accurately capture the initial time period when the thermal response approximates the response of a semi-infinite half plane. If there is not sufficient sampling in this early time, this technique yields inaccurate defect depth estimations. Since determining t_{ps} requires calculating the time derivative of the thermal contrast, estimations of depth from t_{ps} tend to be noisier than estimations based on other timegrams for deep defects.

Future efforts will focus on a curve fitting routine for estimating the thickness from

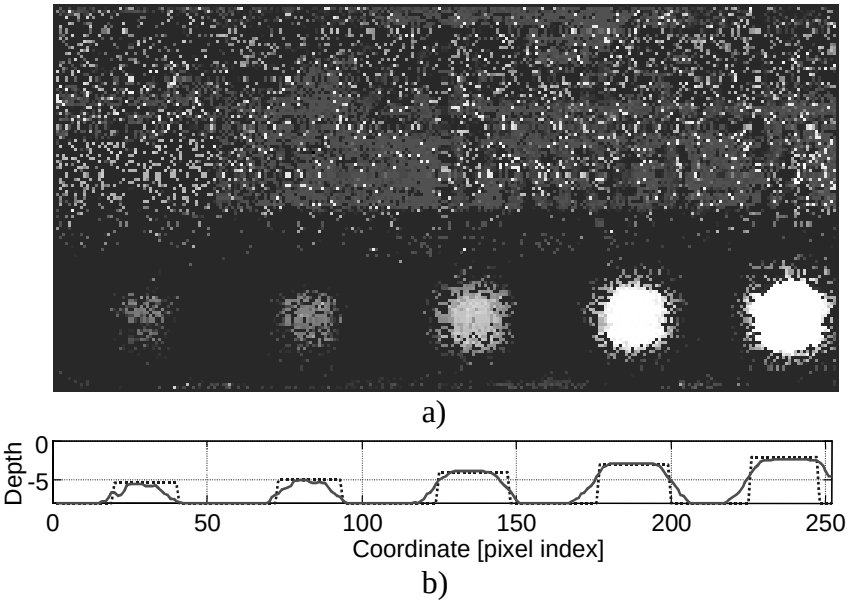

Figure 6. Average depth. a) 2D image; b) depth profile.

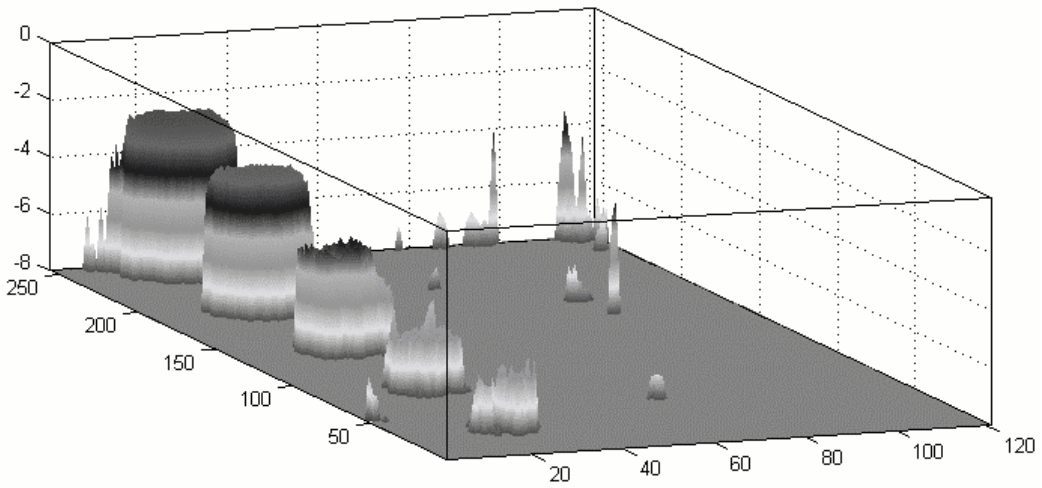

Figure 7. 3D image of the flat bottom holes in the 8-mm composite panel obtained with the thermal technique. Vertical scale is given in mm, horizontal scales are in pixels (approximately 0.86 pixel/mm).

the thermal response in the time interval between t_{div} and $t_{\max}$. Concentrating the analysis on this region may lead to the most robust method for defect depth estimation. This work demonstrates that information on the depth of the defect is present during this entire time interval.

ACKNOWLEDGMENTS

This work was performed while author Plotnikov held a National Research Council - NASA Langley Research Center Associateship

REFERENCES

1. J.-C. Krapez, D. Balages, A. Deom, and F. Lepoutre, in: *Advances in Signal Processing for NDE of Materials*, X. Maldague (ed.), NATO ASI Series, Series E (1994), p. 303.
2. L.D. Favro, Xiaoyan Han, P.K. Kuo, and R.L. Thomas, in *Thermosense XVIII*, Proc. SPIE Vol. 2766, eds. D.D. Burleigh and J.W.M. Spicer (SPIE, Bellingham,1996), p. 236.
3. V. Vavilov, X. Maldague, B. Dufort, F. Robitaille, and J. Picard, NDT & E International, Vol. 26, 2 (1993), p. 85.
4. V. P. Vavilov, in: *Thermosense XVIII*, SPIE Vol. 2766, eds. D.D. Burleigh and J.W.M. Spicer (SPIE, Bellingham, 1996), p. 276.
5. X. Maldague, *Nondestructive Evaluation of Materials by Infrared Thermography*, (Springer-Verlag, London, 1993).
6. W.P. Winfree and K.E. Cramer, in: *Thermosense XVIII*, Proc. SPIE Vol. 2766, eds. D.D. Burleigh and J.W.M. Spicer (SPIE, Bellingham, 1996), p. 228.
7. Y.A. Plotnikov and W.P. Winfree, in: *Thermosense XXI*, SPIE Vol. 3700, eds. D.H. LeMieux, J.R. Snell (SPIE, Bellingham, 1999), p. 26.